Numerical investigation of the role of masonry typology on shear strength

Shenghan Zhang, Katrin Beyer*

Earthquake Engineering and Structural Dynamics (EESD), Institute of Civil Engineering, ENAC, École Polytechnique Fédérale de Lausanne (EPFL), Switzerland

Abstract

The force-displacement behavior of masonry elements depends on the properties of their constituents, mortar and unit, as well as on their typology, i.e., the shape and size of the units and the patterns they generate. Up until now, only few numerical studies investigated the influence of the masonry typology on the mechanical properties of the masonry. The lack of research is caused by both the difficulty of generating specific stone masonry typologies, which vary depending on geographical regions, construction periods, and building technology, and the difficulty of conducting detailed micro-modeling analyses. Building on our recent developments of a typology generator and a detailed micro-modeling method based on cohesive elements, we investigate the relation between masonry typology and maximum shear resistance. After calibration of the model for shear-compression tests, the study examines the validity of Mann and Müller's theory at the nonlinear stage, clarifies the role of the line of minimum trace in characterizing effective interlocking, and investigates the correlation of maximum shear resistance with various indexes. We show that the effect of the interlocking between units on the shear strength is overestimated by the Mann-Müller model. This study provides a fundamental contribution to our understanding of the influence of masonry typology on the masonry shear strength.

*Corresponding author
Email address: katrin.beyer@epfl.ch (Katrin Beyer)

Keywords: historical masonry, stone pattern, line of minimum trace, block area ratio, detailed micro-modeling, force capacity
2010 MSC: 00-01, 99-00

1. Introduction

Masonry is among the oldest construction materials and was used to construct many of today's cultural heritages. Due to the low strength and quasi-brittle behavior of the material, masonry buildings are among the most vulnerable structures under earthquake loading (D'Ayala and Speranza, 2003; Grünthal, 1998). A good understanding of their seismic behavior is required to plan effective strengthening interventions and preserve the appearance and fabric of such cultural heritage. However, understanding the mechanical behavior of masonry elements is a long-standing challenge in civil engineering (Roca et al., 2010). The force displacement behavior of masonry elements depends on the properties of their constituents, mortar and unit, as well as on their typology, i.e., the shape and size of the units, i.e., brick or stone, and the patterns they generate. This paper focuses on the influence of the latter, masonry typology. Masonry typology varies considerably depending on geographical regions, construction periods, and building technology. Up until now, relatively little research has been dedicated to study its influence on the mechanical properties of masonry, especially for irregular stone masonry. Until today, the influence of the masonry typology on masonry strength was mainly studied experimentally, but this approach has its limits due to the large number of masonry typologies that exist and the large costs of experimental tests. Numerical simulations could allow investigation of a large range of masonry typologies provided the model can represent the micro-structures with sufficient detail and can reproduce its mechanical behavior.

When modeling masonry elements, models with three levels of sophistication are normally distinguished, i.e., macro-modeling, simplified micro-modeling, and detailed micro-modeling. Macro-modeling is by far the most common strategy

for engineering practice. It treats masonry as a homogeneous material (Milani, 2011) and often relies on experimental tests to provide necessary information for the constitutive law of the masonry. Methods that can account explicitly for the masonry pattern are the simplified micro-model (Senthivel and Lourenço, 2009; Wilding et al., 2017) and the detailed micro-model (Pina-Henriques, 2005; Vandoren et al., 2013; Zhang et al., 2017). In the former, mortar joints are modeled as zero thickness interface elements while in the latter, mortar, units, i.e., brick or stone, and sometimes also interfaces are modeled explicitly. With the advent of advanced numerical models and the increase of computational power, the detailed micro-modeling approach is becoming more and more popular. The detailed micro-modeling approach is particularly suitable for simulating irregular stone masonry typologies. This paper is based on our previous work on the detailed micro-modeling approach with cohesive elements (the numerical formulation is briefly reviewed in Section 2), which has the advantage of explicitly representing cracks and inter-facial damage.

Apart from the complexity of the simulation technique, another difficulty that hinders studying the influence of the masonry typology is the need to systematically generate masonry patterns. Brick masonry patterns can be readily generated, which facilitated a pioneering study on brick masonry typology (Calderini et al., 2010) in which the diagonal compression strengths with various side loading for different bricks are investigated. The classical mechanical model proposed by Mann and Müller explains the influence of brick masonry typologies on shear resistance, and has been widely used to predict the strength of masonry walls with different unit dimensions (Chaimoon and Attard, 2007; Magenes and Calvi, 1997). However, it has not been validated in the nonlinear range. For stone masonry, generation of masonry typologies is more difficult and previous studies mostly focused on only one specific masonry layout (Zhang et al., 2017; Senthivel and Lourenço, 2009) or on stone masonry with rectangular units (Milani and Lourenço, 2010; Cavalagli et al., 2013). One study that investigated the influence of masonry typology on the seismic response of masonry buildings is by Cundari and Milani (2013), who used multi-step models for the pushover

analysis of in-plane loaded historical masonry walls for a specific irregular stone masonry typology. The structure is simplified as an equivalent frame model, composed by structural members, i.e., piers and spandrels, which are assumed to be elastoplastic. The maximum resistance of each structural member is estimated by limit analysis upper bound finite element approach and is influenced by the masonry typology.

Several research groups have studied the influence of masonry typology experimentally in recent years. Vasconcelos and Lourenço (2009) have conducted shear-compression tests on three different typologies. Almeida et al. (2012) studied the compressivecyclic behavior of masonry wall with different textures. In these studies, masonry typology was shown to have a significant influence on the masonry mechanical behavior. However, the relation between masonry typology and masonry strength is still not clear. Though the Line of Minimum Trace (LMT) (Almeida et al., 2016; Calderini et al., 2010; Doglioni et al., 2009) is proposed to quantitatively characterize stone masonry typologies and used as an input when determining Masonry Quality Index (MQI) which has been correlated to masonry shear strength (Borri and De Maria, 2009). No previous study has investigated numerically and quantitatively the correlation between the texture of stone masonry and its shear resistance.

In this study, after calibrating our detailed micro model with Vasconcelos and Lourenço (2009)'s tests on "irregular masonry" (Section 4), we start our investigation with analyzing regular masonry typologies. For the first time, the classical model by Mann and Müller is examined for the nonlinear force-displacement behavior of masonry. More specifically, it is investigated whether the key assumptions of the model by Mann and Müller hold at maximum shear resistance(Section 5). The influences of unit aspect ratio, bond pattern, mortar thickness and size effect are considered. To transit to irregular stone masonry, we further study the influence of the unit shape, changing from rectangular to ellipse, by which the essential conditions for effective interlocking are discussed (subsection 5.4). For stone masonry, we investigate the correlation between

maximum shear resistance and various indexes, including LMT. The most important findings are recapitulated in the conclusion section (Section 6).

2. Numerical framework

The finite element analysis is conduced with the open source library Akantu (Richart and Molinari, 2015). The numerical framework has been introduced in Zhang et al. (2017) and is only briefly reviewed in this section.

After spatial discretization based on finite elements, we can obtain the following well-known relation

$$\mathrm{M}\,u + F^{\mathrm{int}} = F^{\mathrm{ext}} \tag{1}$$

where M represent the mass matrix, u is the vector indicating acceleration, F^{ext} represents external load, and F^{int} indicates internal forces.

For time integration, the second order central difference method is adopted, based on which the displacement u_{m+1}, velocity $\underline{u}_{m+1}$, acceleration u_{m+1} of time step $m+1$ is estimated by quantities at time step m

$$u_{m+1} = u_m + t\_u_m + \frac{1}{2}t^2 \quad u_m \tag{2}$$

$$u_{m+1} = \mathrm{M} \quad ^1(F^{\mathrm{ext}}_{m+1} \quad F^{\mathrm{int}}_{m+1}) \tag{3}$$

$$\underline{u}_{m+1} = \underline{u}_m + \frac{1}{2}t(\ u_{m+1} + u_m) \tag{4}$$

To ensure stability, the following restriction for time step needs to be satisfied

$$t < \quad \frac{l_e}{c} \tag{5}$$

in which t is the constant time step, c is the longitudinal wave speed, l_e is the characteristic length of the minimum element, is a safety factor, chosen to be 0:15 here.

In this study, we assume that material nonlinearity only comes from cohesive elements (Ren and Li, 2012) while an isotropic elastic relation is used for bulk elements. F^{int} is calculated by the spatial integration of stresses within bulk elements and tractions within cohesive elements, for which an extrinsic cohesive

zone model (Camacho and Ortiz, 1996) is used here, which means cohesive elements are not present in the mesh when the simulation begins and cohesive elements will be inserted once the stress exceeds the threshold (Camacho and Ortiz, 1996).

$$\sigma^{effc} > \sigma_c \tag{6}$$

where σ_c indicates the material tensile strength, σ^{effc} is a norm calculated from the stress state (Camacho and Ortiz, 1996).

After insertion, the mechanical behavior of cohesive elements is governed by the traction-separation law. In this study, we adopted the traction-separation law proposed by Snozzi and Molinari (2013), for which

$$T = (T_s; T_n) = \begin{bmatrix} 2 & 0 \\ 0 & 1 \end{bmatrix} \begin{bmatrix} \tau_t; \sigma_n \end{bmatrix} \frac{T}{\sigma} \tag{7}$$

where T_s and T_n are two components of traction T in the tangential direction s and the normal direction n of the cohesive element, respectively. The parameter β represents the ratio of fracture energies of Mode II and Mode I, i.e., $\beta = G_{c;II}/G_{c;I}$, indicates the ratio between cohesion (shear strength) and tensile strength and T is a scalar norm determined by cohesive opening from a linear traction-separation law (Snozzi and Molinari, 2013).

3. Typology generator and line of minimum trace

As indicated in the introduction, one corner stone which was missing when investigating masonry typologies is the ability to systematically generate stone patterns for each typology. To address this problem, we recently proposed a typology generator (Zhang et al., 2018a). One illustrative example is shown in Figure 1. The construction of the masonry typology can be divided into two stages, i.e., the construction of a joint pattern (Figure 1a), and an erosion process to create the mortar layer (Figure 1b). With different parameters, the generator is able to create different typologies. Typical samples for five typologies in the Italian code are shown in Figure 2 (Zhang et al., 2018a).

One parameter to differentiate masonry typologies quantitatively is the Line of Minimum Trace (LMT) (Almeida et al., 2016; Calderini et al., 2010; Doglioni

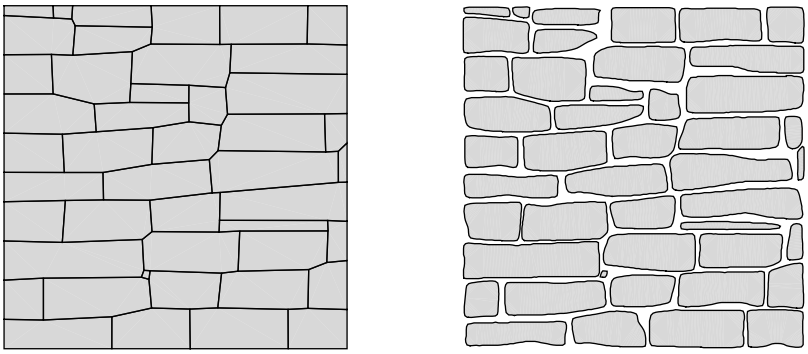

(a) a joint pattern (b) after erosion process

Figure 1: Examples of stone patterns generated by the typology generator

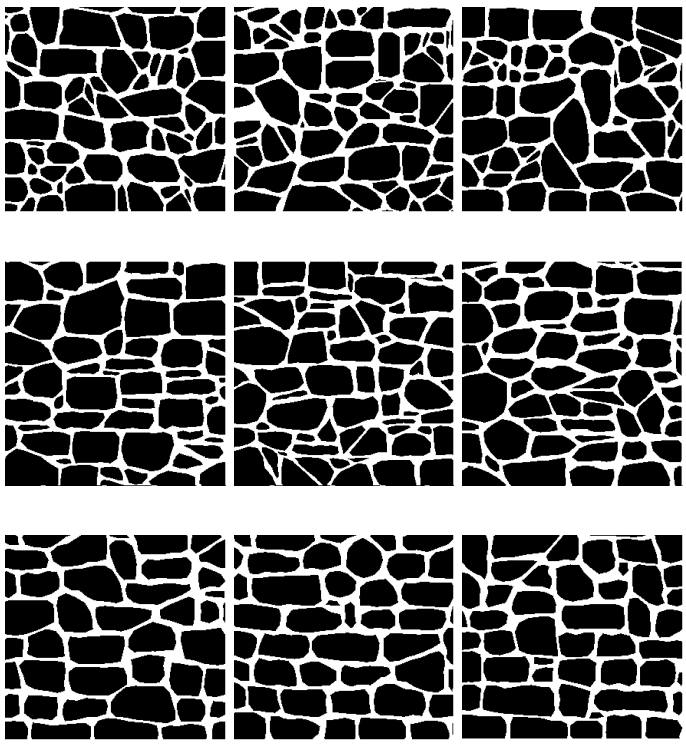

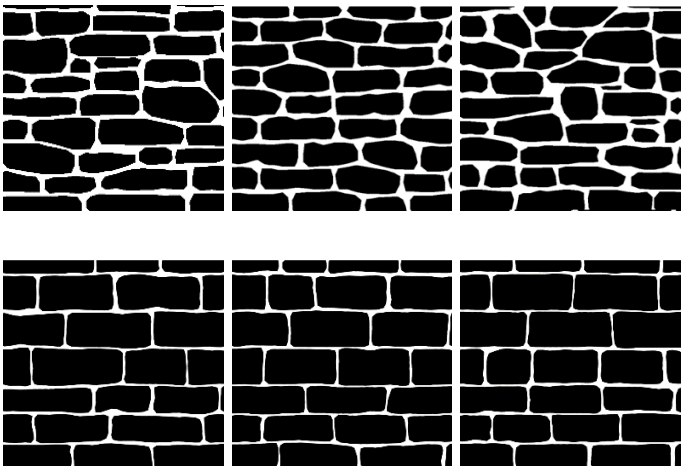

Figure 2: Generated samples for five typologies of the Italian code.

et al., 2009), which characterizes the degree of interlocking between stones. The generalized definition of the LMT is (Zhang et al., 2018a)

$$\text{LMT} = \frac{\min(\quad \text{distance along the edge} + \text{distance through the mortar})}{\text{direct distance between two points}} \tag{8}$$

in which is the index representing the difference between the interface and mortar strength. The traditional LMT is computed for = 1 and for a vertical base line. However, the diagonal direction is also used (Calderini et al., 2010). For the example in Figure 1, the two LMTs for different -values are illustrated below in Figure 3.

An index for characterizing the irregularity of the shape of the stones is the block area ratio, defined by the ratio of unit area with regard to the smallest bounding box around the stone. The block area ratio is thus defined by

$$\text{block area ratio} = \frac{\sum_i A_s^i}{\sum_i A_b^i} \tag{9}$$

in which A_s^i is the area of stone i and A_b^i is the area of the minimum bounding box. An illustration example is shown in Figure 4, in which the red rectangles are minimum bounding boxes for the stones. The stones touching the edge are not considered to eliminate boundary effect.

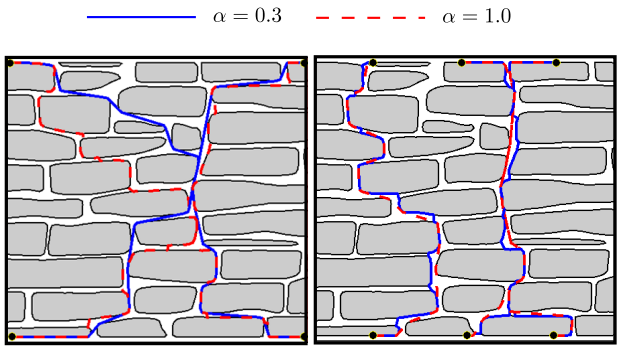

Figure 3: Indicating line of minimum trace

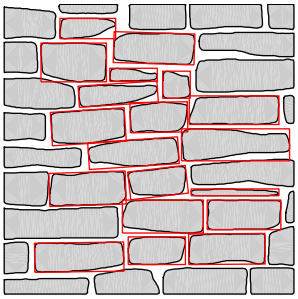

Figure 4: Illustrating bounding boxes of the stones

Though LMT has been put forward to quantitatively characterize the masonry typology, no previous study has investigated the correlation between LMT and masonry strength. The correlation between different indexes and maximum shear resistance will be investigated in Section 6. The code for generating different masonry typologies, calculating LMT, and transforming pictures to FEM mesh is publicly available on c4science(https://c4science.ch/diffusion/5485/).

4. Calibration of the model for shear-compression test

The proposed numerical model has been validated for shear tests in Zhang et al. (2018b), diagonal compression tests in Zhang et al. (2017), and compression tests in Zhang et al. (2018a). To further validate the model, we simulate shear-compression tests by Vasconcelos and Lourenço (2009) on irregular stone masonry walls.

In this test series, the wall is subjected to cycles of horizontal top displacement while the compression load on the wall is maintained constant throughout each test. Vasconcelos and Lourenço (2009) tested seven different walls of irregular stone masonry under three different compression levels, i.e., 0.500 MPa (two walls), 0.875 MPa (three walls), and 1.250 MPa (two walls). The load is introduced by a loading beam on top of the wall. The rotation is free at the top of the loading beam and the wall is therefore tested under cantilever boundary conditions. Since the numerical model has not yet been validated for cyclic loading, we compare the simulation results only with the envelope of experimental force-displacement relation in Figure 5. We use for all walls the same micro-structure, for which the mesh is constructed by transforming the schematic drawing in Figure 1b in Vasconcelos and Lourenço (2009) into a Gmsh file using a Matlab routine we have developed in Zhang et al. (2018a). Senthivel and Lourenço (2009) constructed a mesh without mortar for a simplified micro-modeling analysis and obtained a good agreement between the numerical simulation results and the experimental results. One difficulty faced by advanced simulations is the determination of material properties, e.g., Senthivel and Lourenço (2009) adjusted the elastic stiffness of interfaces to fit the experimental results.

The material properties used in our simulation are listed in Tables 1 and 2. Table 1 lists the values assumed for the Young's modulus E, the Poisson's ratio $\square$ and the density $\square$ for unit and mortar, while Table 2 includes information on the tensile strength f_t, the cohesion c, the fracture energy associated to first mode of fracture G_c^{I} and to the second mode G_c^{II} as well as the friction

coefficient □ for cohesiveelements. Apart from the limited information provided by experiments, as shown in Table 1, we make the following assumptions: (1) the mortar is assumedto be 3 times stronger than the interface (Zhang et al., 2017); (2) the ductility index $G_c^{\mathrm{I}}=f_t$ is chosen to be the same as in Senthivel and Lourenço (2009); (3) the ratio of $G_c^{\mathrm{II}}=G_c^{\mathrm{I}}$ is set to be 10; (4) for the friction coefficient, a typical value of 0.5 is selected for mortar and interface; (5) the cohesion is assumed to be 1.5 times stronger than the tensile strength. Based on those assumptions, the material properties are selected by choosing a value for f_t, which leadsto a good match of the numerical simulation results with the experimental observation in terms of maximum force capacity of the walls.

It should be noted that evenunder the samecompressionand for the samety-pology, a large discrepancy is observed among experimental force-displacement relations, e.g., the coefficient of variations for peak strengths of experimental tests are 5%, 13%, and 5% for compression 0:500MPa, 0:875MPa, 1:250MPa, respectively. This variability is typical for the strength of stone masonry walls Vanin et al. (2017). Part of this difference comes from the slightly different stone layouts between the walls and the variation of material properties across the masonry panel (Zhang et al., 2017). For the sake of simplicity and due to lack of more detailed information, we assumehere that all walls have the same layout and the material properties are uniform acrossthe specimen. While comparing the simulation results with experiments, we plot both loading directions in the same plot, i.e., we do not distinguish between the loading directions. Each subfigure shows therefore two curves representing numerical results obtained for loading in the positive and negative direction and four or six courses representing envelopes from experimental testing (four curves for $\square_N$ = 0.500 and 1:250MPa for which two walls each were tested, and six curves for $\square_N$ = 0:875MPa for which three walls were tested). Note, to better represent the simulation results, here a Blackman window is applied to the force-deform curve to eliminate high frequency content. It can be seenthat there is a relatively good match between the simulation results and the experimental results.

Figure 6 compares the failure modes obtained from simulation to the crack patterns observed in the experiments. The figure shows that the failure modes change with the compression level. Under low compression (0.500 MPa), the specimen displays a flexural failure (Figure 6a). With higher compression (0.875 MPa, 1.250 MPa), shear cracks start to dominate the failure mode (Figure 6c, e). It should be noted that, similar to the force displacement relation, the

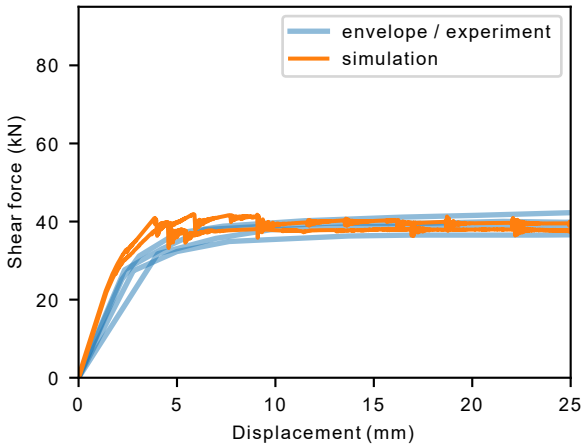

(a) compression 0.500 MPa

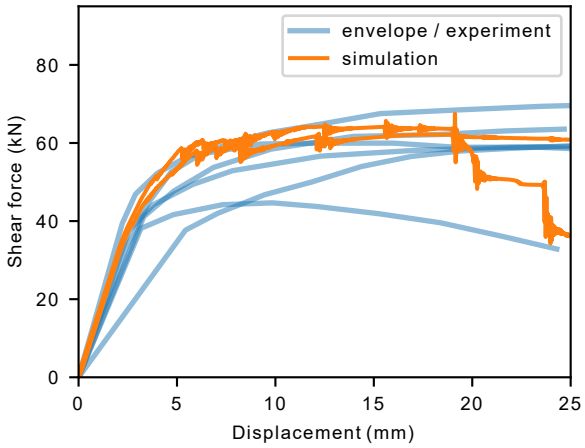

(b) compression 0.875 MPa

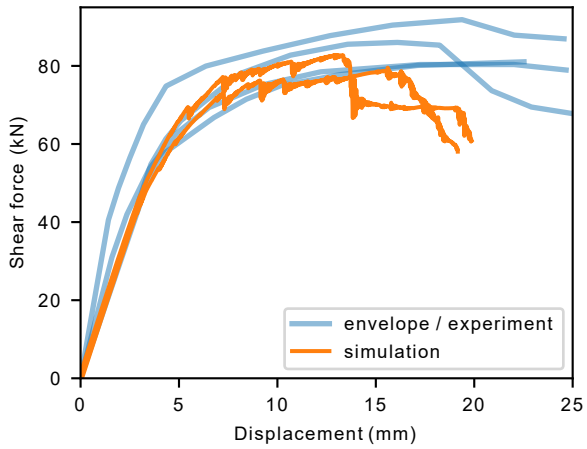

(c) compression 1:250MPa

Figure 5: Comparing the numerical simulation results with envelopsof hysteresiscurves from experiments

Table 1: Simulation of shear-compressiontests by Vasconcelosand Lourenço (2009): Assumed elastic properties for unit and mortar

	E (MPa)	□	□ (kg=m^3)
unit	20 200[a]	0.2[a]	2 600[b]
mortar	170	0.2	1 800

[a] Parameter taken from Senthivel and Lourenço (2009)
[b] Parameter taken from Vasconcelosand Lourenço (2009)

Table 2: Simulation of shear-compressiontests by Vasconcelosand Lourenço (2009): Assumed inelastic properties for unit, mortar and interface

	f_t (MPa)	c (MPa)	G_c^{I} (N=m)	G_c^{II} (N=m)	□
unit	2.00	4.00	2 000	20 000	0.75
mortar	0.60	0.90	120	1 200	0.5
interface	0.20	0.30	40	400	0.5

crack patterns observed for specimens tested at the same compression level are not identical (Vasconcelos and Lourenço, 2009). Considering the similarity in micro-structure among different specimens, the difference is most likely caused by the spatial variation of material properties, as demonstrated in Zhang et al. (2017).

The comparison in Figures 5 and 6 shows that our model based on cohesive elements well captures the failure modes for shear-compression test. In the following section, we further investigate the relation between the masonry typology and shear strength.

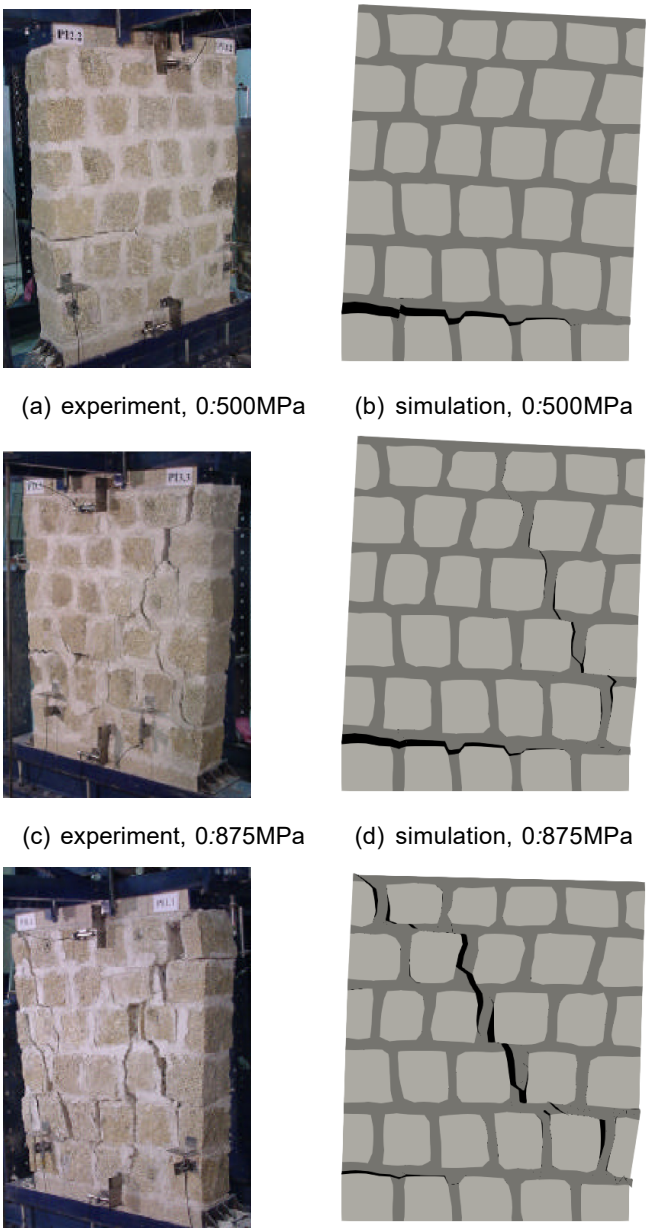

(a) experiment, 0:500MPa (b) simulation, 0:500MPa

(c) experiment, 0:875MPa (d) simulation, 0:875MPa

(e) experiment, 1:250MPa (f) simulation, 1:250MPa

Figure 6: Comparison of typical crack pattern: left, experiments Vasconcelos(2005); right, simulation.

5. Understanding the influence of interlocking through variation of masonry typologies

Up to now, the most widely accepted explanation for interlocking is the well-known Mann and Müller's theory (Mann and Müller, 1982; Calderini et al., 2010), which is developed for brick masonry and is based on the following assumptions

1. The stress transfer via head joints is negligible.
2. The shear stress is uniformly distributed along the bed joint; the compressive stress is uniform along the overlapping length between two units.
3. The strength of the wall is predicted by the stress state at one "point", more precisely, the stress state of one overlapped joint considering assumption 2. Stress redistribution caused by nonlinear material properties is not considered.

The possibility of brick failure is omitted here for simplicity, by setting a relatively high strength and fracture energy for the brick. Following these assumptions, the stress distribution on one brick is shown in Figure 7, which also illustrates the double bending boundary condition of the masonry wall, which is used for the numerical simulations, and the dimensions of the unit and the specimen. In Figure 7, □ = 2*h*/*l* indicates the influence of interlocking, with *h* and *l* being the height and width of the unit. Following Figure 7, the shear resistance predicted by Mann and Müller's theory is

$$\square = \frac{c}{1+\square\square} + \frac{\square}{1+\square\square}\square_y \tag{10}$$

in which *c* is the cohesion and □ is the friction coefficient of the bed joints, usually evaluated through the triplet test (Zhang et al., 2018b).

Due to the difficulties of performing detailed micro-modeling analysis, no previous study has validated Mann and Müller's theory in the nonlinear range. In the following part of this section, we evaluate the accuracy of Equation 10 by comparing FEM simulation results for different unit sizes and different material parameters (subsection 5.1). To further investigate the role of interlocking,

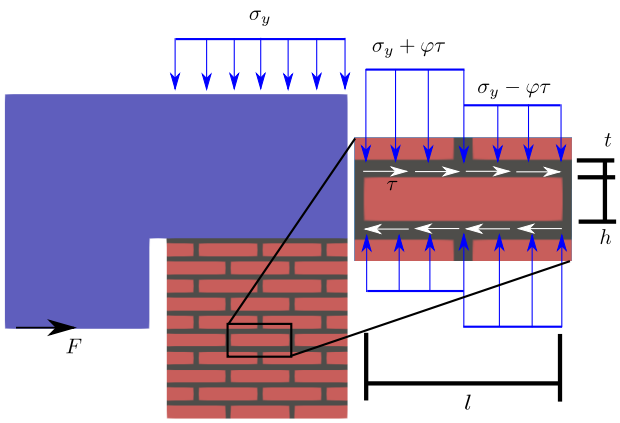

Figure 7: Stress distribution on one brick that is assumed in Mann and Müller's model

Table 3: Parametric study on masonry typology: Elastic properties of unit and mortar

	E (MPa)	□	□ (kg=m^3)
unit	20 200[a]	0.2[a]	2 600[b]
mortar	500	0.2	1 800

we alter the bond pattern to examine its influence on masonry shear strength (subsection 5.2). With the help of a parallel computing framework, a much larger wall size can be the simulated and we will also briefly discuss the effect of the wall size on the masonry shear strength. All previous discussion is based on rectangular units, representing brick masonry. To transit to stone masonry, we further study how the masonry strength is influenced by the unit shape (subsection 5.4).

The numerical framework used has been summarized in Section 2. The boundary condition used was introduced in Figure 7. The base material properties are presented in Tables 3 and 4 (Zhang et al., 2018a).

The simulations are mainly conducted on the cluster Deneb at EPFL. This high-performance computing cluster has 376 nodes with two Ivy Bridge octo-cores processors running at 2:6 GHz, and 64 GB of DDR3 RAM. For the FEM

Table 4: Parametric study on masonry typology: Inelastic properties of unit, mortar and interface

	f_t (MPa)	c (MPa)	G_c^{I} (N=m)	G_c^{II} (N=m)	□
unit	1.00[b]	2.00	1 000[b]	10 000	0.5
mortar	0.15	0.30	30	300	0.5
interface	0.05[a]	0.10[a]	10	100[a]	0.5

mesh, 6 node second order plane strain elements are used. The loading rate is 0:005ms ^{1} and the simulation time depends on the specimen size. For instance, for the largest specimen in this study, illustrated by the Figure 15c, the mesh contains 207^{0}639 elements. The simulation takes 2 days while using 4 nodes in Deneb (64 cores).

5.1. Influence of the unit aspectratio

For the test setup in Figure 7, and with the material properties in Tables 3 (compared with Table 1, only the mortar elastic modulus has changed) and 4 (compared with Table 1, the assumptions (1), (2), (3), (4) are kept, we further assume that *=beta* is 2 and f_t for interface is 0:05MPa), the force-deformation curves, under different compression levels, □$_N$ = 0:1, 0:5, 0:9 MPa, are presented in Figure 8. The shear strength of the wall, i.e., the maximum shear resistance, corresponds to the highest point of the curve, as indicated in Figure 8.

Figure 9 investigates the influence of the unit length, changing from l = 0:24 to 0:106 and 0:0525 m, on the shear strengths; these unit lengths correspond to unit length over unit height ratios of l/h = 4:6 to 2:0 and 1:0, respectively. The four different subfigures present the results for different sets of material parameters: the first three subfigures vary the nonlinear material properties, i.e., □ = 0:5, G_c^{I} = 10 N m ^{1} for Figure 9a, □ = 0:5, G_c^{I} = 1 N m ^{1} for Figure 9b and □ = 0:8, G_c^{I} = 10 N m ^{1} for Figure 9c, while Figure 9d modifies the elastic properties of the unit to be more representative of brick masonry, i.e., density □ = 1994kg m ^{3}, elastic modulus E =16 700MPa and Poisson's ratio □ = 0:15 (Zhang et al., 2018b). In these plots the continuous lines represent

the estimation according to Mann and Müller and the markers the simulation results. We can deduce from the figure: (1) As a first estimation, Mann and Müller's model matcheswell with the simulation results; (2) Mann and Müller's model overestimates the effect of interlocking; For instance, if we consider a compression level 0:5 MPa and the material parameters □ = 0:8 and G_c^{I} = 10 N m ^{1} (Figure 9b), for a decreaseof l/h from 4:6 to 1:0, Mann and Müller's theory predicts a decreaseof 39% for the maximum shear resistance, while the actual decreaseis only 20%. (3) The nonlinear material parameters, which are not considered by Mann and Müller's model, e.g., the fracture energy, do have a non negligible effect on the shear strength. For instance, for l/h = 4:6 and □ = 0:5, with fracture energy drops from 10 N m ^{1} to 1 N m ^{1}, the shear strength decreasesby 15%, 8%, 10% for compression levels of 0:1 MPa, 0:5 MPa, 0:9 MPa, respectively; (4) Modification of the unit properties has negligibly effects on the simulation results. Comparing Figure 9a and Figure 9d with different unit properties, the mean error of the maximum shear resistances is 1%, while the largest error is 3%. The small difference comesfrom the fact that in either case,the unit is much stiffer comparedto the mortar, which alsofulfills the assumption of Mann and Müller.

To facilitate the discussion, we focus on only one compression level $□_N$ = 0:5 MPa with □ = 0:5, G_c^{I} = 10 N m ^{1} in the following sections. The shearstrengths for different situations, e.g., different arrangementsof the units, different mortar thicknessesand variation of unit shapes,are summarized in Figure 10. The three blue circles in Figure 10 are the same points in Figure 9a under compression 0:5 MPa. Other points in Figure 10 will be discussedin the following sections.

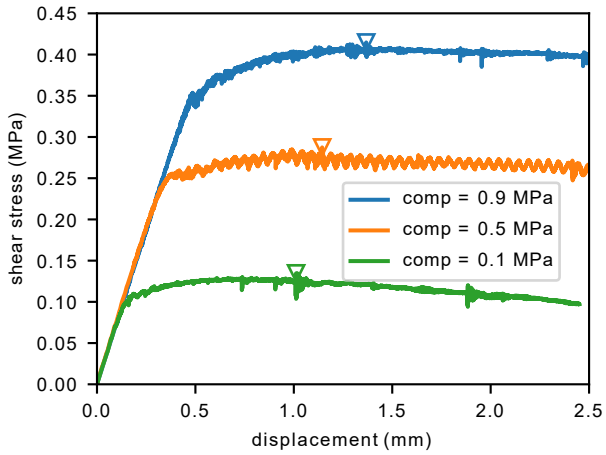

Figure 8: Force displacement relations for different compression levels for unit shape $l/h = 4.6$

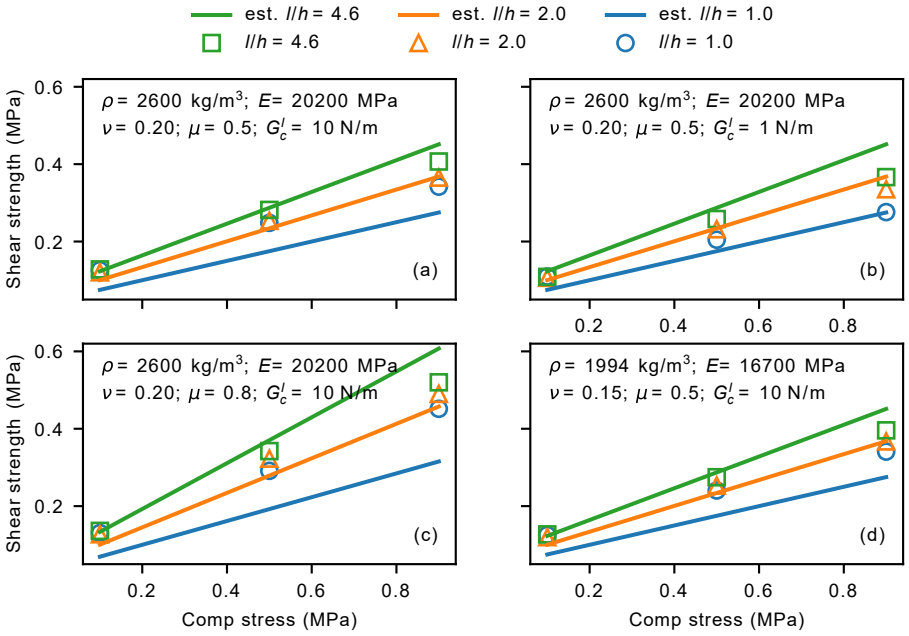

Figure 9: Comparing simulation results with Mann and Müller's model for different material parameters

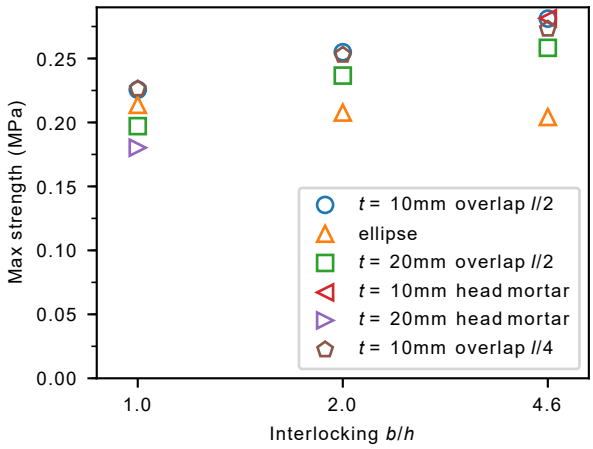

Figure 10: Influence of mortar thickness, bond pattern and shape of the units on maximum shear strength. Simulation results are for shear-compression tests under double bending and with a mean compression stress of σ_N = 0:5 MPa.

5.2. *Influence of the bond pattern and mortar thickness*

As shown in the previous section, the fracture energy has a non negligible effect on the masonry shear strength and is neglected by Mann and Müller's model. Another parameter that is also neglected by Mann and Müller's model is the mortar thickness. For historical masonry, this is of particular relevance, because the mortar thickness varies considerably from case to case. By doubling the mortar thickness from t = 10 mm to t = 20 mm, the shear strength drops by 12%, 7%, 8%, for unit shapes of l/h = 1:0, 2:0, 4:6, respectively.

In Mann and Müller's model, the stress transfer via the head joints is neglected. In previous simulations, material properties for bed mortar and head mortar are assumed to be the same. To investigate the influence of the head joint mortar, we reduce the elastic modulus of the head joint mortar to 1=10 of that of the bed joint mortar and repeat the analyses for two masonry typologies, i.e., for l/h = 4:6, t = 10 mm and for l/h = 1:0, t = 20 mm. For the first masonry typology, where the unit is long and the mortar is thin, the maximum shear resistance is hardly influenced by the head joint properties, while for the

latter situation, where the unit is square and the mortar is thick, thus more representative for stone masonry, the maximum shear resistance decreases by 9% for the reduced elastic modulus of the head joint mortar. This suggests that for detailed micro-modeling of historical stone masonry, the effect of the head joint mortar needs to be considered, while for brick masonry, the head joint mortar does not influence the results significantly.

We then investigate the three assumptions of Mann and Müller's model. For comparison, apart from running bond with overlapping distance l=2, we investigate another bond pattern with overlapping distance l=4. The two typologies are shown in Figure 11. We indicate four sections in Figure 11 along which the stress distribution will be investigated. The stress distributions along the four sections in Figure 11 are plotted in the four subfigures of Figure 12. The compression stress and shear stress at two different loading stages are presented, i.e., for an elastic stage at around half the maximum resistance indicated with solid lines, and at maximum resistance indicated with dashed lines. To better view the relation between stress distribution and unit arrangements, the position of each cross section examined is illustrated again near the x-axis of the corresponding subfigure. According to the prediction by Mann and Müller's model, the compressive stress will follow a stair-stepped distribution (the length of each stair step is half the length of the brick), asymmetric along the two adjacent cross sections, as illustrated in Figure 7, while the shear stress is assumed to be uniform.

Directly from Figure 12, we can conclude that: (1) The key assumption of Mann and Müller's theory (assumption 2) is valid within the elastic range for both bond patterns; (2) At maximum resistance, the shear stress is no longer uniformly distributed along the brick length, i.e., the part with lower compressive stress also sustains a lower level of shear stress, suggesting a stress redistribution before reaching the maximum resistance; (3) Both the shear stresses and the compression stresses decrease at the center of the sections, where the sections cross the diagonal crack. The crack pattern of the masonry wall with overlapping distance of l=4 is shown in Figure 13; (4) While Mann and Müller's

theory can be extended to bond patterns with overlapping length *l*=4, the failure criterion, assumption 3, is overly conservative, because the shear stress along the *l*=4 overlapping length decreased significantly at maximum shear resistance, which suggests that it failed at an early stage. This is further illustrated by the deformation at maximum resistance in Figure 13, in which the *l*=4 overlapping part has already detached. This conclusion shows that any extension of Mann and Müller's theory to bond patterns different to running bond or extension to stone masonry, needs to reconsider the failure criterion.

The error of extending Mann and Müller's theory to other bond patterns while still preserving the form in Equation 10 with □ = $\frac{h}{l}$, in which *l* is the overlapping length, can be quantitatively examined. For running bond, we have □ = $\frac{2h}{l}$, while for an overlapping length of *l*=4, we obtain □ = $\frac{4h}{l}$. With the parameters listed in Table 4, while the typology changes from Figure 11a to Figure 11b, the extended Mann and Müller's model will predict a decrease of 25% for maximum shear resistance. The actual difference of the maximum shear resistances for the two situations in Figure 11 is within 1%, as indicated in the force-displacement relation in Figure 14. The third bond pattern included in the figure is the stack bond pattern, indicated by overlapping distance 0. Compared with the other two bond patterns, the shear strength of stack bond is 8% lower. What significantly distinguishes the stack bond from the other two bond patterns is the early deviation of the force-displacement curve from the elastic prediction, e.g., the effective stiffness measured by 70% of the maximum resistance is 55% lower than the stiffness of the running bond masonry.

For other brick dimensions, i.e., *l*/*h* = 1:0 and 4:6, we examine the same bond pattern with overlapping length *l*=4. Although there is a significant difference of LMT between overlapping length *l*=4 and overlapping length *l*=2, the shear strengths of the walls under overlapping length *l*=4 are almost identical to those for running bond (Figure 10), which suggests that the LMT is not sufficient for correlating the bed joint strength with the masonry shear strength.

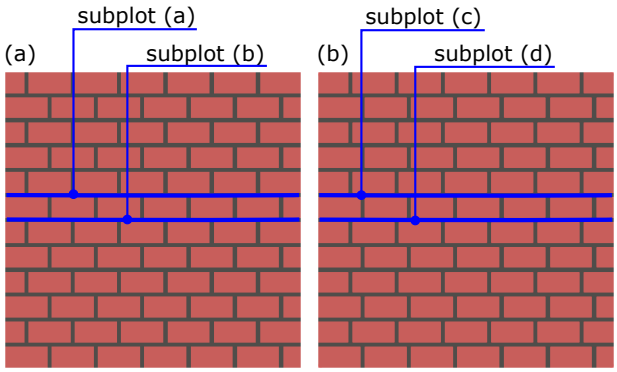

Figure 11: Comparison of bond patterns: overlapping length *l*=2 (a) and overlapping length *l*=4 (b) and positions of cross sections for stress distributions in Figure 12

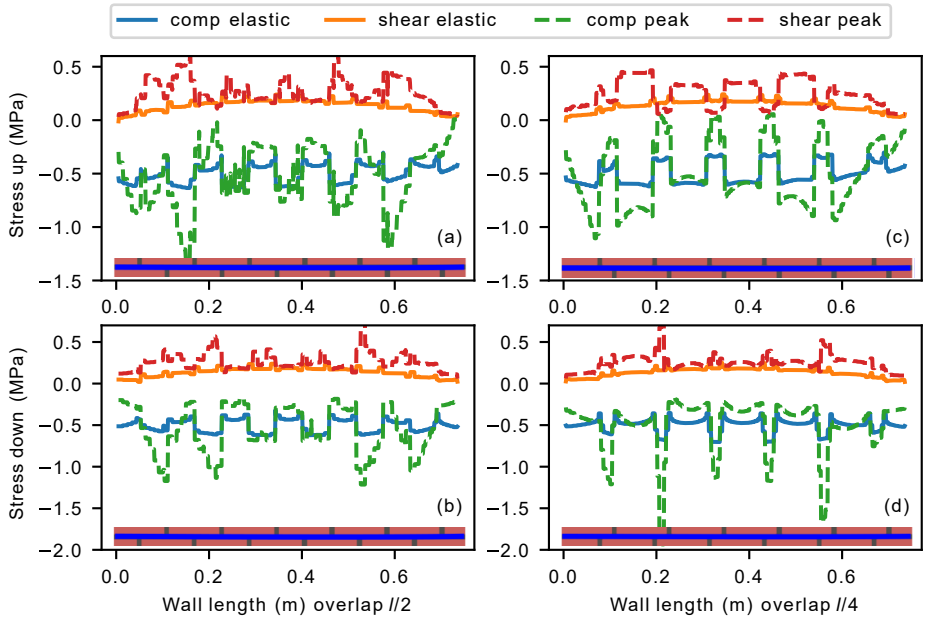

Figure 12: Comparison of stress distributions at elastic stage and maximum strength for different bond patterns

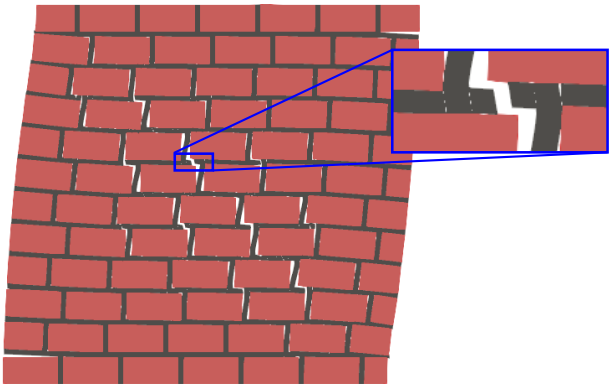

Figure 13: Deformation for overlapping length *l*=4 at maximum shear resistance

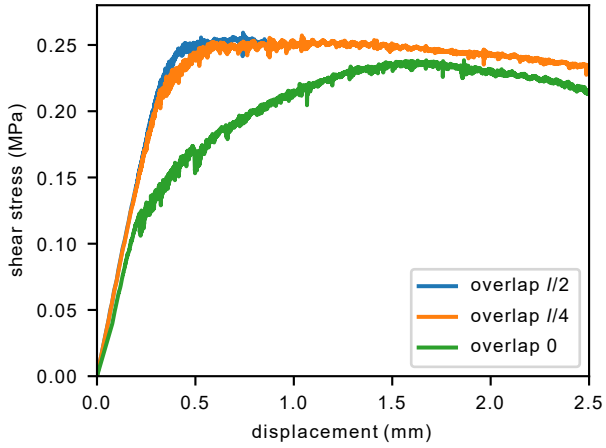

Figure 14: Force displacement relation for different overlapping lengths

5.3. Influence of the size effect

Another factor that influences the masonry strength, which has not been considered in previous studies, is the size effect. There are three factors that play a role with regard to the size effect:

1. The ratio of fracture energy with regard to the wall size. This effect has been well studied and discussed for mode I fracture of quasi-brittle material, e.g., concrete (Bazant and Planas, 1997).
2. The relative size of the brick with regard to the wall size. For the same brick dimension, the larger the wall size, the more homogeneous the material is.
3. If randomness is considered, the relative size of the correlation length of the random field with regard to the wall size.

Three wall sizes, 0.79 m, 1.49 m and 2.99 m, are considered, as illustrated in Figure 15. The unit shape considered is l/h = 4.7. To simplify our discussion, the material property is assumed to be constant as in Tables 3 and 4. Therefore only the first two factors listed above are considered in the discussion.

Figure 16 compares the maximum shear resistances for three wall sizes. The shear resistance of the wall gradually increases with the decrease of the wall size. More specifically, while the wall size decreases from 2.99 m to 0.79 m, the wall strength increases by 14%. This suggests that the experimental tests that are conducted on small walls will overestimate the strength of large walls found in real buildings. Note that this conclusion needs to be verified for 3D structures with large sliding algorithm.

Homogenized simulations for masonry are built on the assumption that as the size of the specimen gets larger, the stress will be more and more uniformly distributed. For the wall size 0.79 m, the stress distributions along the two intersections in the middle, indicated in the Figure 11a, are presented in Figure 12a, b, respectively. For convenience of comparison, Figure 17 represents again the stress distribution for wall size 0.79 m and also shows the stress distribution for the wall size 2.99 m.

As shown in Figure 17: (1) with the increase of the wall size from 0.79 m to 2.99 m, the stress distribution along a chosen cross section becomes smoother, especially the shear stress distribution; (2) for both wall sizes, the stress distribution along the wall length changes significantly after the elastic range and the

stress distribution at peak strength is much less uniform than the stress distribution in the elastic range (Figure 12 and Figure 17), e.g., both shear stress and compression stress decrease at the center of the section; (3) despite the large wall size considered (2.99 m), there is still not a region within the wall where the stress is approximately uniform over an area considerably larger than the unit size, which indicates that treating masonry as a homogeneous material might introduce errors.

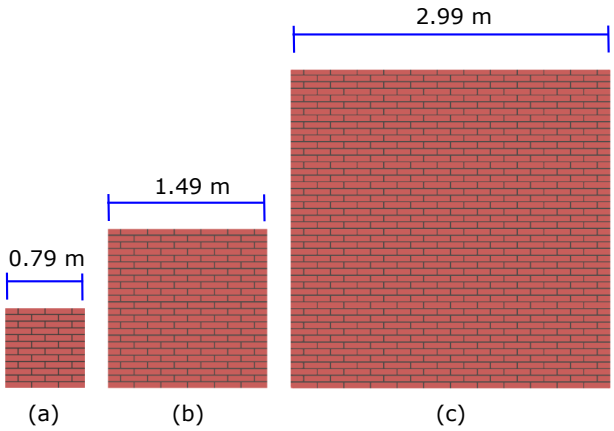

Figure 15: Illustration of different wall sizes

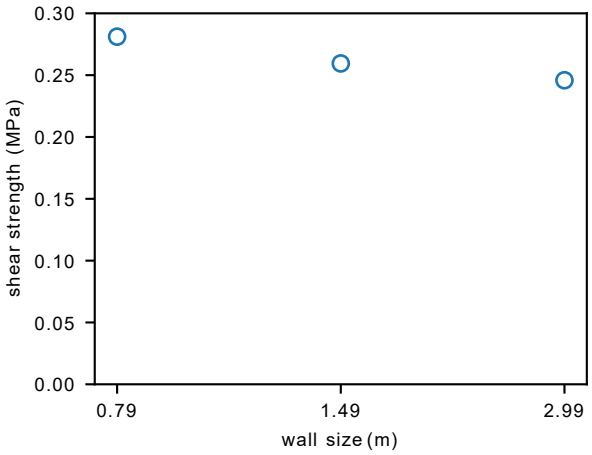

Figure 16: Maximum shear resistances for different wall sizes

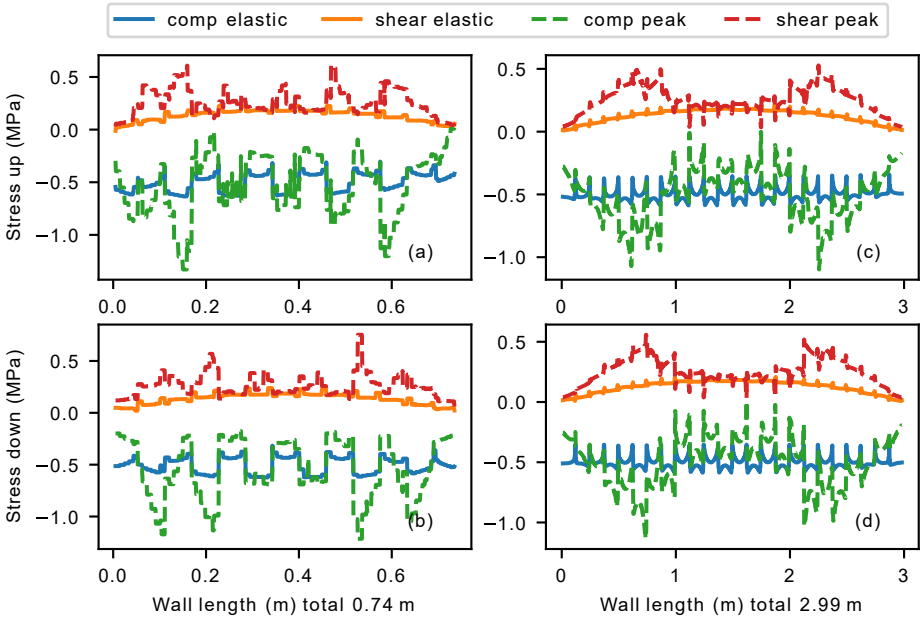

Figure 17: Comparison of stress distributions at the elastic stage (solid lines) and the point of maximum strength (dashed lines) for different wall sizes

5.4. Influence of the unit shape: from rectangular to ellipse

The previous discussions on masonry typology are based on rectangular units, representing brick masonry. For stone masonry, however, the shapes of units vary considerably. To study the effects of unit shape, we analyze the variation of maximum shear resistance when the unit shape changes from rectangular to ellipse in this section.

Starting from the rectangular patterns in the first row of Figure 18, we construct the corresponding elliptic patterns in the second row, following two rules: (1) the ratio of major axis to minor axis of the ellipse $a=b$ is kept the same as the ratio of unit dimension $l=h$; (2) for each row of ellipses, the minimum distance is 10 mm, while the distance between two adjacent rows are determined to keep the ratio of mortar area to unit area the same as in the corresponding rectangular typology. Figure 18 also shows the mesh resolution we used for representing the different masonry typologies. It can be seen that the mesh is rather fine and the masonry typology is well represented by the mesh resolution.

The maximum shear resistances of the rectangular patterns in Figure 18 are indicated by "t =20 mm overlap l=2" in Figure 10, while the elliptic patterns are indicated by "ellipse". With $l=h$ changes from 1:0 to 4:6 for rectangular pattern, the maximum shear resistance increases by 31%. For elliptic pattern, however, the maximum shear resistance decreases by 4% when $a=b$ increases from 1:0 to 4:6. Despite the large difference of LMT for elliptic patterns, the maximum shear resistances are similar, which confirms the previous conclusion that the LMT alone does not characterize well the interlocking between stones. At the same time, the different trends for rectangular and elliptic patterns also indicate that the unit shape is essential in establishing an effective interlocking. The similarity of maximum shear resistances for square unit pattern $l=h$ = 1 and sphere unit pattern $a=b$ = 1, illustrated by the left column of Figure 18, suggests a lack of interlocking for square unit pattern, which shows that effective interlocking also depends on the ratio $l=h$.

For the long unit ($l=h$ = $a=b$ = 4:7), the maximum shear resistance of the patterns shown in the third column of Figure 18 differs by 21% (Figure

10). To study the transition process, we gradually change the unit shape from rectangular to ellipse, as illustrated in Figure 19, in which the mortar thickness is determined by the two rules given above. In Figure 19, the block area ratio is used (Section 3) to quantity the unit shape, e.g., for rectangular units, the block area ratio is obviously 1:00, and for elliptical units, it is ($\pi ab/4$)=(ab)= 0:79. The maximum shear resistances are plotted against the block area ratio in Figure 20. The results indicate a significant correlation between block area ratio and the masonry maximum shear resistance.

To further interpret the interlocking effect, we plot the compression stresses on the brick surfaces at maximum shear resistance for four different unit shapes in Figure 21. According to Mann and Müller's theory, for running bond masonry, there is a vertical alternation of the compression stress, in other words, there are diagonal compression bands forming through the bricks. This effect is clearly seen in the subplot (a) of Figure 21. With the decrease of the block area ratio from 1:00 to 0:79, this effect is less and less obvious, i.e., the compression struts become more and more vertical.

The crack patterns at the maximum shear resistance are shown in Figure 22. While for rectangular units, the flexural cracks are still visible at the two corners of specimen, for elliptic unit, the deformation is purely shear. Since the flexural resistance is independent of the masonry typology, as will be confirmed in the next section, the difference of the crack patterns suggest a lower shear resistance for elliptic unit, caused by the lack of effective interlocking.

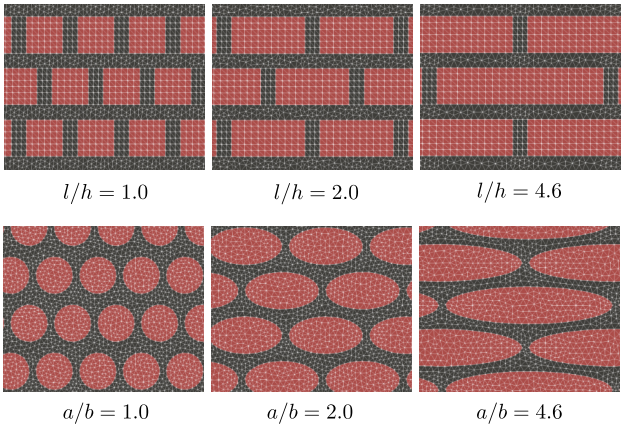

Figure 18: Comparison of rectangular unit and elliptic unit

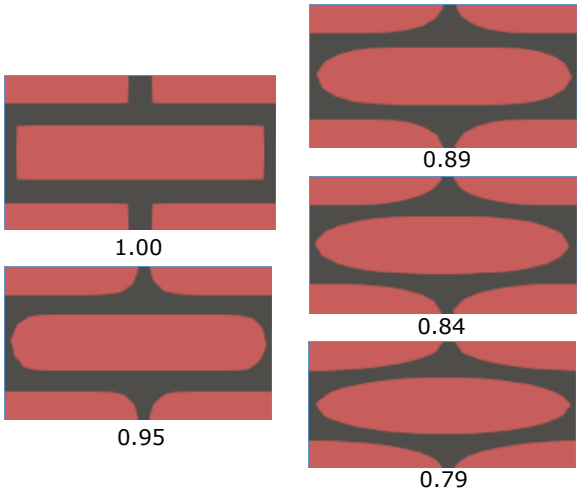

Figure 19: Changing from rectangular to ellipse

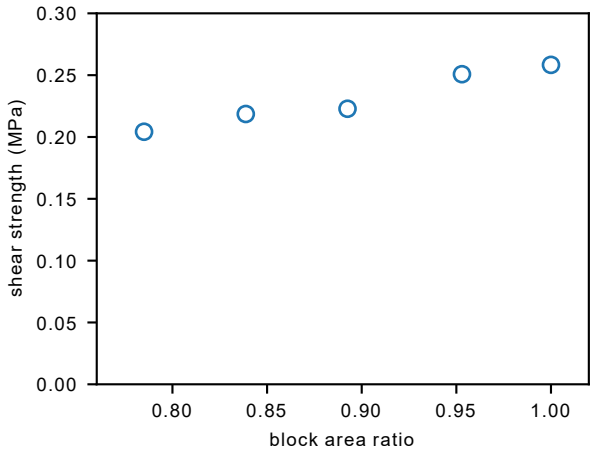

Figure 20: Maximum shear resistance with regard to block area ratio

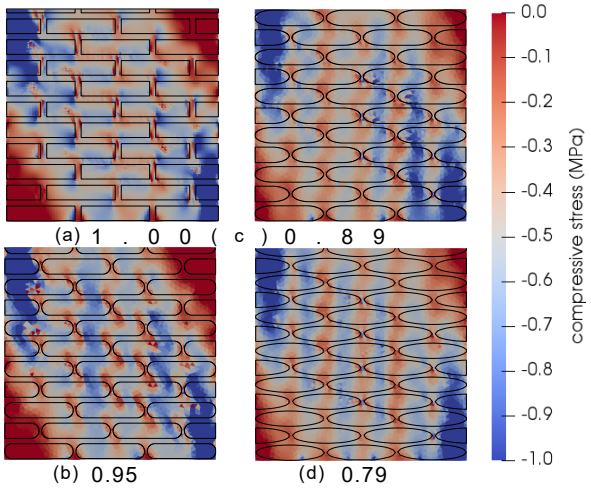

Figure 21: Compressive stress for different masonry patterns

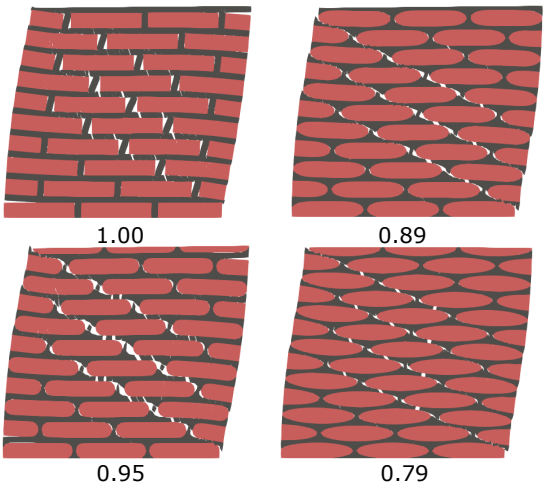

Figure 22: Deformation at maximum shear resistance for different masonry patterns

6. Correlation between maximum shear resistance and various indexes

In this section, we examine the maximum shear resistances of the different stone masonry typologies shown in Figure 2 for different boundary conditions. We then investigate the correlation between maximum shear resistances and typical indexes for stone masonry, i.e., the LMT in vertical/diagonal direction and the block area ratio. The material properties are those given in Tables 3 and 4. Apart from the double bending boundary condition illustrated in Figure 7, we further consider a cantilever boundary condition. As in previous sections, three different compression levels are applied: σ_N = 0.1 MPa, 0.5 MPa, and 0.9 MPa. Because the stone masonry specimens are asymmetric, for each boundary condition and for each compression level, two loading directions are considered, i.e., from left to right and from right to left. In total, 90 FEM analyses are conducted.

Typical crack patterns for each typology and each compression level are shown in Figure 23 for the cantilever boundary condition and in Figure 24 for the double bending boundary condition. All crack patterns are plotted for

the point of maximum shear resistance. The left column of each figure shows the crack patterns for the lowest compression level (0.1 MPa) and the right column those for the highest compression level (0.9 MPa). For both boundary conditions, we see a gradual transition from flexural dominated damage to shear dominated damage with increasing compression level (i.e. from left to right). For high compression, shear cracks dominate the failure modes for both boundary conditions (right column in Figures 23 and 24).

For each boundary condition and for each compression level, five different indexes are computed, i.e., LMT measured in the vertical direction (with = 0.3 and = 1.0, illustrated in Figure 3), LMT measured in the diagonal direction (with = 0.3 and = 1.0, illustrated in Figure 3) and the block area ratio (illustrated in Figure 4). The maximum shear resistances are plotted against the different indexes in Figure 25 for the cantilever boundary condition, and in Figure 26 for the double bending boundary condition. Indicated in each plot are Pearson's linear correlation coefficient and the coefficient of determination r^2.

From Figures 25 and 26, we find that: (1) When the wall fails in shear, the boundary condition has a smaller influence on the shear strength than if the walls fails in flexure. For a compression level of 0.5 MPa, the shear strength increases by 22% when the boundary condition changes from cantilever to double-bending (12% increase for compression level 0.9 MPa). Under low compression 0.1 MPa, since the flexural strength is determined by the flexural moment, the shear resistance doubles, from 0.06 MPa to 0.12 MPa while the boundary condition changed from cantilever to double bending boundary condition. (2) For a low compression level $_N$ = 0.1 MPa, there is no linear correlation between maximums shear resistance with any index. This is explained by the fact that the specimens exhibit a flexural failure and the flexural strength is not influenced by the masonry typology but is only dependent on the wall geometry and static and kinematic boundary conditions. (3) For higher compression levels of $_N$ = 0.5 MPa and 0.9 MPa, the shear failure starts to prevail (Figures 23 and 24). There is a positive correlation between maximum masonry shear re-

sistances and all indexes investigated, which also suggests a positive correlation between those indexes. (4) Among all the indexes, the LMT in the diagonal direction with = 0:3 gives the best correlation. The block area ratio is also a good indicator of the maximum shear resistance. Note that the differences among the points of one subfigure are purely caused by the differences between the micro-structures of the various masonry typologies. The imperfect correlation between the geometrical indexes, i.e., LMTs and block area ratio, and the shear strength shows that the here investigated geometrical indexes cannot characterize masonry typology completely.

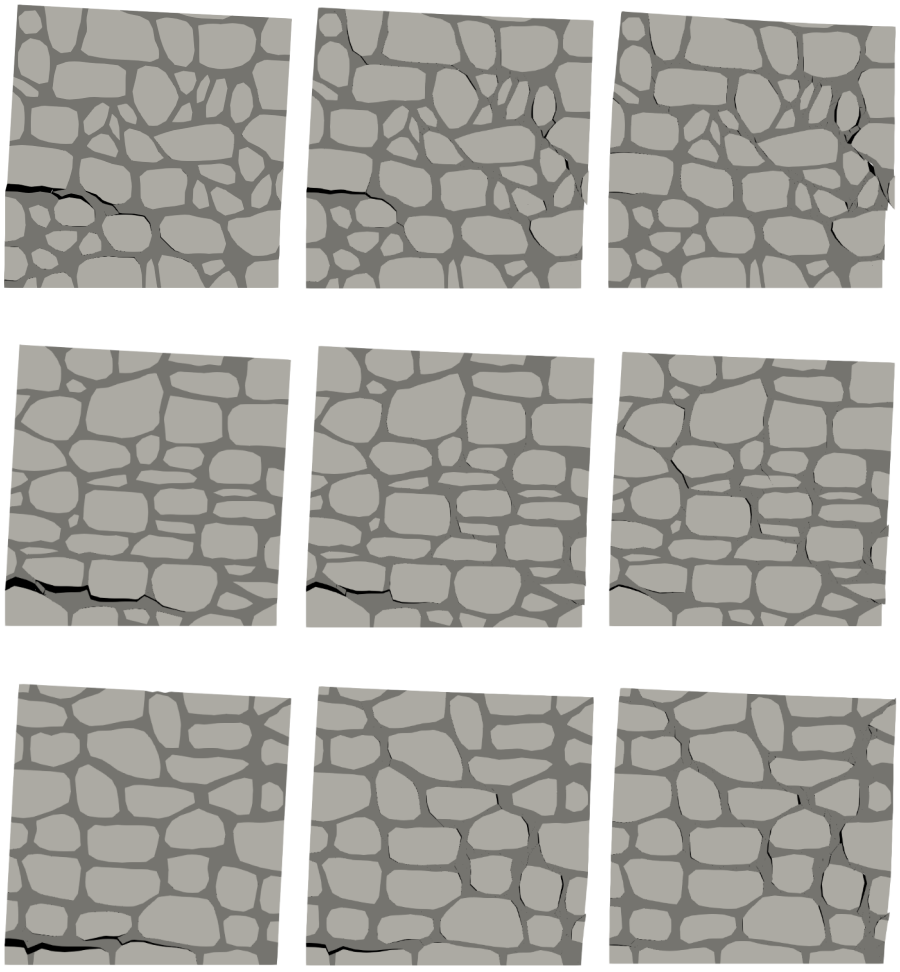

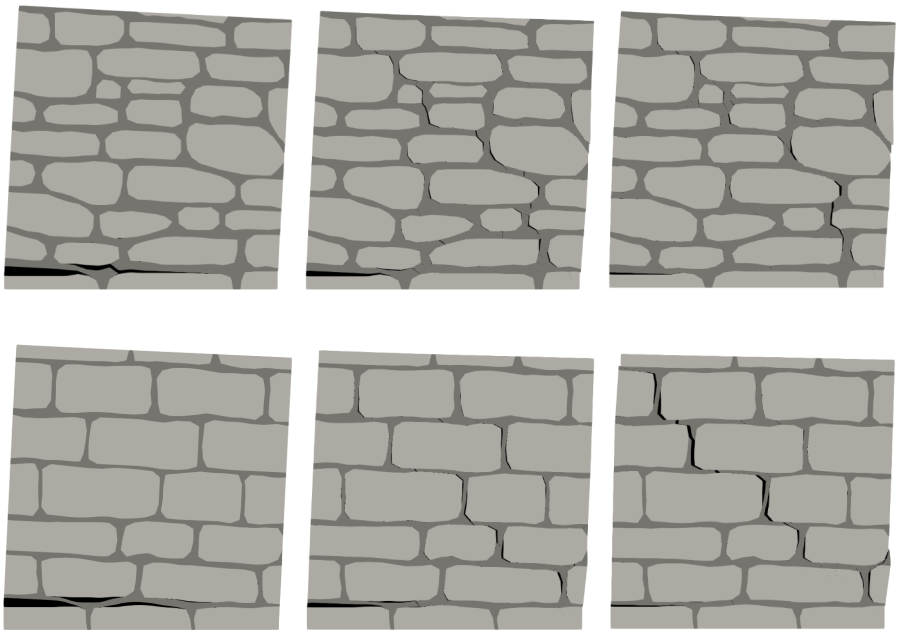

Figure 23: Typical crack patterns for cantilever boundary condition: left, 0:1MPa; middle, 0:5MPa; right, 0:9MPa.

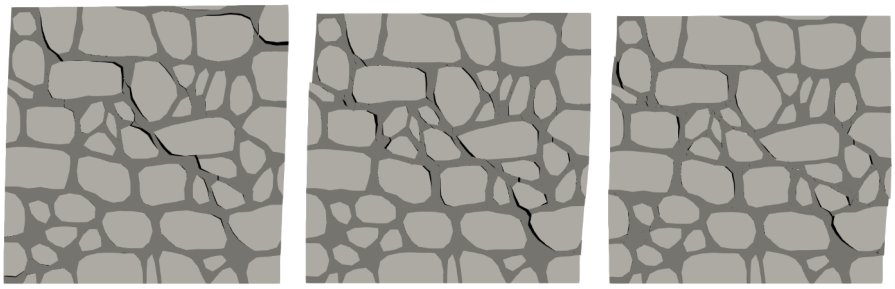

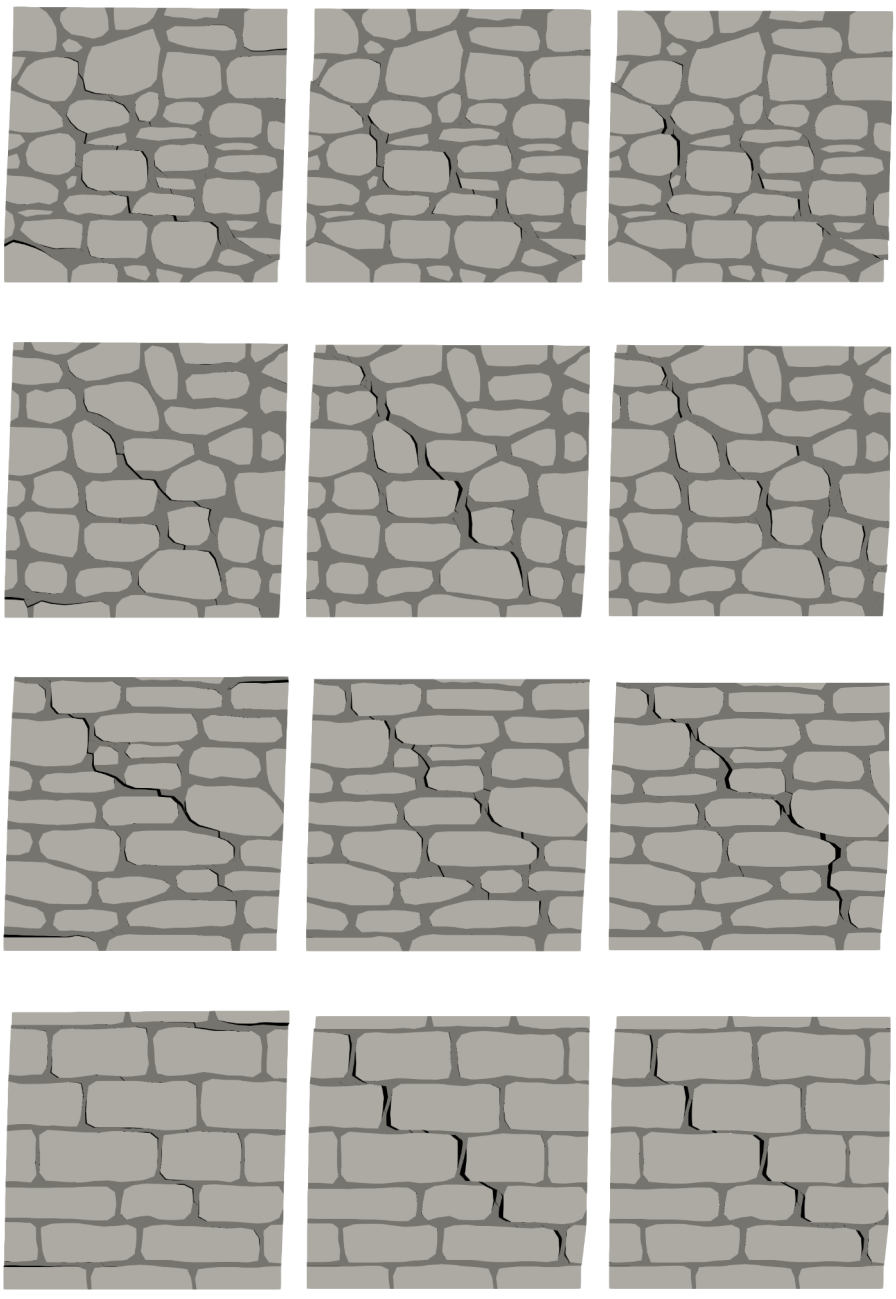

Figure 24: Typical crack patterns for double bending boundary condition: left, 0:1MPa; middle, 0:5MPa; right, 0:9MPa.

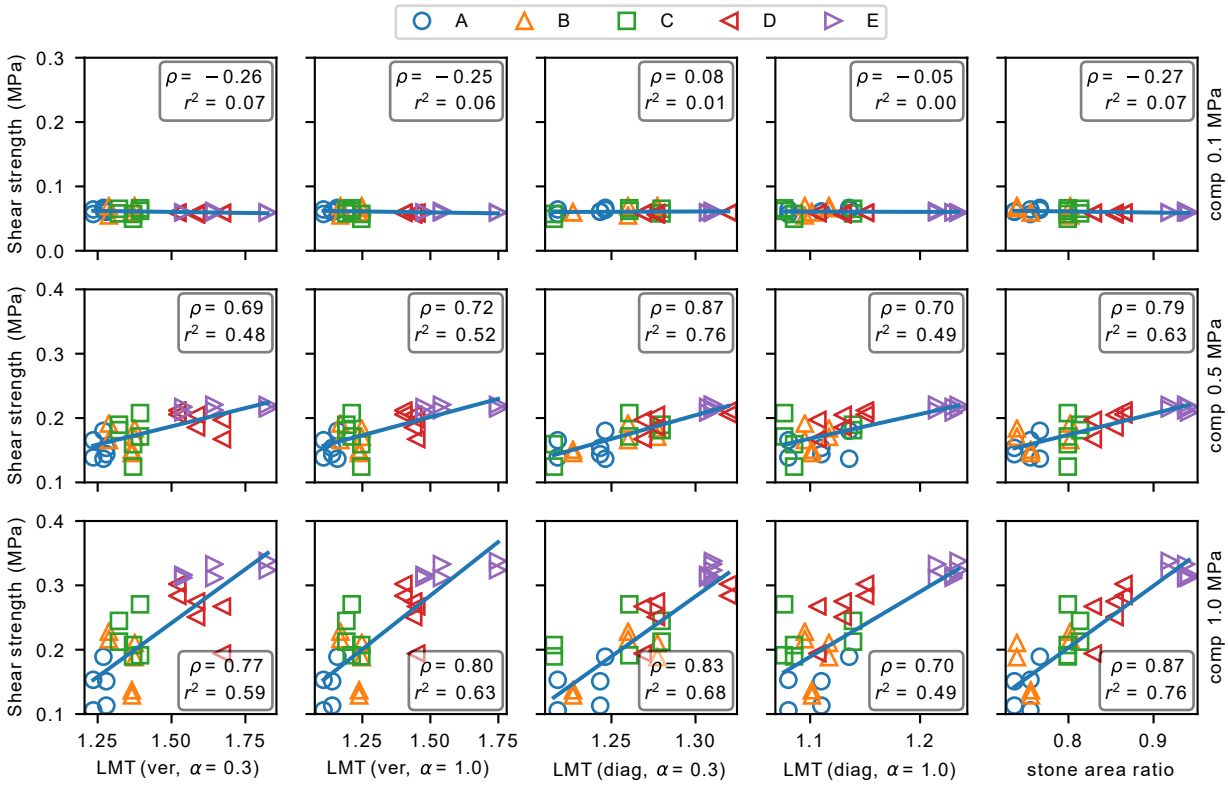

Figure 25: Correlation of shear strength with different indexes for cantilever boundary condition

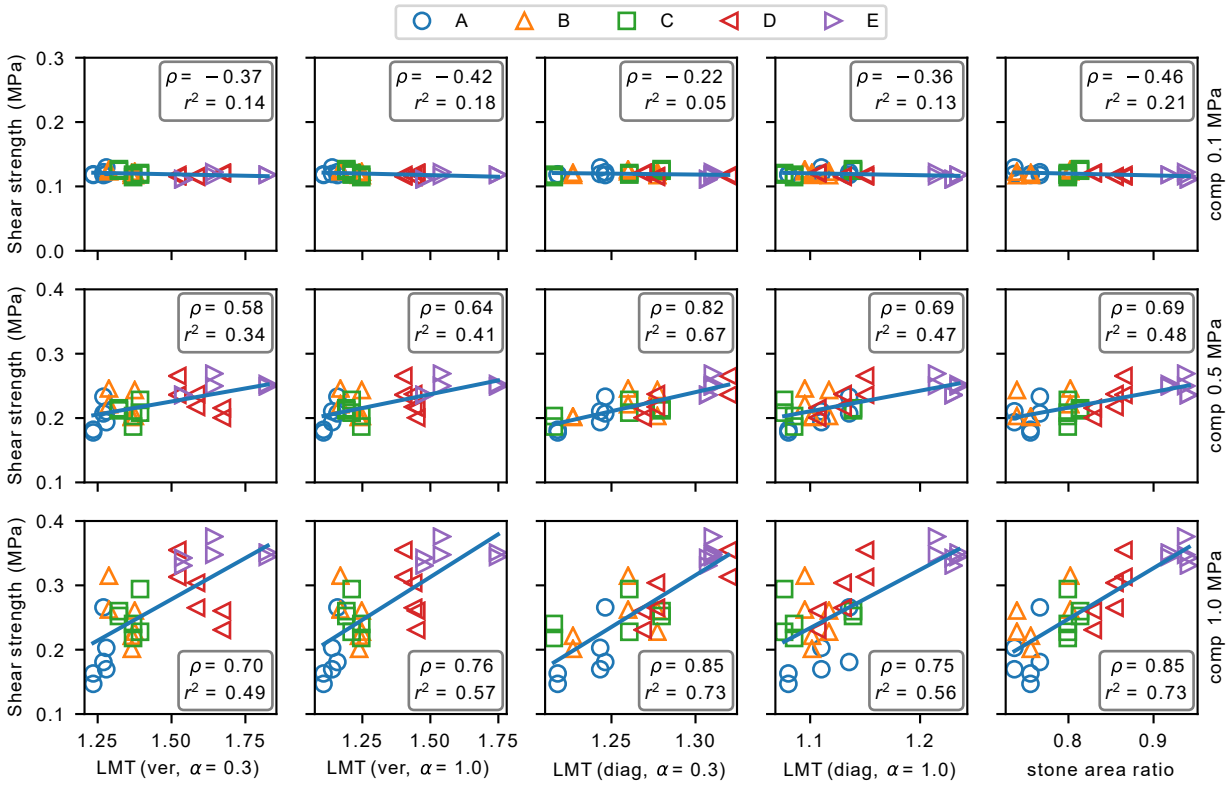

Figure 26: Correlation of shear strength with different indexes for double bending boundary condition

7. Conclusion

The main objective of the current study is to investigate the influence of the masonry typology on masonry shear resistance. Traditionally, the effect of interlocking is interpreted by Mann and Müller's theory. By conducting nonlinear analysis based on a detailed micro-model with cohesive elements, this study shows that: (1) Mann and Müller's main assumption, that the shear stress is constant along the bed joint holds for the elastic stage but is not valid any more at maximum shear resistance. (2) Though Mann and Müller's model gives a reasonable estimate of the shear strength, it overestimates the influence of interlocking. (3) Extension of Mann and Müller's model, to bond patterns other than running bond or to stone masonry, requires careful examination, because the failure of part of the joint does not necessarily indicate reaching the maximum shear resistance. It was found that shear stresses are redistributed along the brick length (comparison between the stress distributions at elastic stage and at maximum shear resistance in Figures 12 and 17). (4) Parameters which are not included in Mann and Müller's model, i.e., mortar thickness, fracture energy, specimen size, do have a significant influence on the shear resistance of masonry.

Mann and Müller's theory has been developed for brick masonry. For stone masonry, the LMT has been widely used as a quantitative indicator for the interlocking between stones. Contrary to the intuition, we show in this study: (1) a high value of the LMT does not guarantee high interlocking, as suggested by the study of different bond patterns in Section 5.2, and also supported by the similarity of shear resistances while the unit shape changes from circle and ellipse in Section 5.4, from which only moderate changes of shear strength were observed despite the large differences in LMTs. The unit shape also has a considerable effect on interlocking, which can be quantified by the block area ratio. It should be also noted that, in reality, masonry built with units close to rectangles also tends to have a larger LMT. (2) For stone masonry, different indexes, LMT and block area ratio, are often positively correlated. (3) For

stone masonry, LMT does show a positive correlation with shear strength, while flexural strength is independent of typology indexes. For this study, the best correlation with the masonry shear strength is obtained for the diagonal LMT with = 0:3. The block area ratio also shows also a strong correlation with the masonry shear strength.

Several questions still remain to be answered. One question is the relation between deformation capacity and the masonry typology. As shown in Figure 14, from running bond to stacking bond, though the shear strengths are relatively similar, there is a large difference with regard to the force-deformation curve. Another unanswered question is the size effect caused by random fields, which is neglected in the current study. Provided the same correlation length, a larger size wall will indicate a higher probability to have a weaker region, which will possibly weaken the masonry strength, thus further intensify the size effect.

8. Acknowledgments

This study was supported by the Swiss National Science Foundation through the grant 200021_140973=1.

References

Almeida, C., Guedes, J. P., Arêde, A., Costa, A., 2016. Geometric indices to quantify textures irregularity of stone masonry walls. Construction and Building Materials 111, 199–208.

Almeida, C., Guedes, J. P., Arêde, A., Costa, C., Costa, A., 2012. Physical characterization and compression tests of one leaf stone masonry walls. Construction and Building Materials 30, 188–197.

Bazant, Z. P., Planas, J., 1997. Fracture and Size Effect in Concrete and Other Quasibrittle Materials. CRC Press.

Borri, A., De Maria, A., 2009. L'indice di qualità muraria (IQM): Evoluzione ed applicazione nell'ambito delle norme tecniche per le costruzioni del 2008. In:

Proceedings of 13th Italian national conference for earthquake engineering. Bologna, Italy.

Calderini, C., Cattari, S., Lagomarsino, S., 2010. The use of the diagonal compression test to identify the shear mechanical parameters of masonry. Construction and Building Materials 24 (5), 677–685.

Camacho, G. T., Ortiz, M., 1996. Computational modelling of impact damage in brittle materials. International Journal of Solids and Structures 33 (20), 2899–2938.

Cavalagli, N., Cluni, F., Gusella, V., 2013. Evaluation of a statistically equivalent periodic unit cell for a quasi-periodic masonry. International Journal of Solids and Structures 50 (25-26), 4226–4240.

Chaimoon, K., Attard, M. M., 2007. Modeling of unreinforced masonry walls under shear and compression. Engineering Structures 29 (9), 2056–2068.

Cundari, G. A., Milani, G., 2013. Homogenizedand heterogeneouslimit analysis model for pushover analysis of ancient masonry walls with irregular texture. International Journal of Architectural Heritage 7 (3), 303–338.

D'Ayala, D., Speranza, E., 2003. Definition of collapse mechanisms and seismic vulnerability of historic masonry buildings. Earthquake Spectra 19 (3), 479–509.

Doglioni, F., Mirabella Roberti, G., Bondanelli, M., 2009. Definizione della Linea di Minimo Tracciato come elemento per la qualifica dell'ingranamento nel piano e fuori dal piano, RELUIS project, Final report of work package1. Tech. rep.

Grünthal, G., 1998. European Macroseismic Scale 1998 (EMS-98). Tech. rep.

Magenes, G., Calvi, G. M., 1997. In-plane seismic response of brick masonry walls. Earthquake Engineering & Structural Dynamics 26 (11), 1091–1112.

Mann, W., Müller, H., 1982. Failure of shear-stressed masonry – an enlarged theory, tests and application to shear-walls. In: Proceedings of the British Ceramic Society. London.

Milani, G., 2011. Simple homogenization model for the non-linear analysis of in-plane loaded masonry walls. Computers & Structures 89 (17–18), 1586–1601.

Milani, G., Lourenço, P. B., 2010. Monte carlo homogenized limit analysis model for randomly assembled blocks in-plane loaded. Computational Mechanics 46 (6), 827–849.

Pina-Henriques, J., 2005. Masonry under Compression: Failure Analysis and Long-Term Effects. Ph.D. thesis, University of Minho.

Ren, X., Li, J., 2012. Dynamic fracture in irregularly structured systems. Physical Review E 85 (5), 055102.

Richart, N., Molinari, J.-F., 2015. Implementation of a parallel finite-element library: Test case on a non-local continuum damage model. Finite Elements in Analysis and Design 100, 41–46.

Roca, P., Cervera, M., Gariup, G., Luca, P., 2010. Structural analysis of masonry historical constructions. Classical and advanced approaches. Archives of Computational Methods in Engineering 17 (3), 299–325.

Senthivel, R., Lourenço, P. B., 2009. Finite element modelling of deformation characteristics of historical stone masonry shear walls. Engineering Structures 31 (9), 1930–1943.

Snozzi, L., Molinari, J.-F., 2013. A cohesive element model for mixed mode loading with frictional contact capability. International Journal for Numerical Methods in Engineering 93 (5), 510–526.

Vandoren, B., De Proft, K., Simone, A., Sluys, L. J., 2013. Mesoscopic modelling of masonry using weak and strong discontinuities. Computer Methods in Applied Mechanics and Engineering 255, 167–182.

Vanin, F., Zaganelli, D., Penna, A., Beyer, K., 2017. Estimates for the stiffness, strength and drift capacity tests reported in the literature. Bulletin of Earthquake Engineering 15 (12), 5435–5479.

Vasconcelos, G., 2005. Experimental Investigations on the Mechanics of Stone Masonry: Characterization of Granites and Behavior of Ancient Masonry Shear Walls. Ph.D. thesis, University of Minho, Guimaraes.

Vasconcelos, G., Lourenço, P. B., 2009. In-plane experimental behavior of stone masonry walls under cyclic loading. Journal of Structural Engineering 135 (10), 1269–1277.

Wilding, B. V., Dolatshahi, K. M., Beyer, K., dec 2017. Influence of load history on the force-displacement response of in-plane loaded unreinforced masonry walls. Engineering Structures 152, 671–682.

Zhang, S., Hofmann, M., Beyer, K., 2018a. A 2D typology generator for historical masonry elements. Construction and Building Materials (184), 440–453.

Zhang, S., Richart, N., Beyer, K., 2018b. Numerical evaluation of test setups for determining the shear strength of masonry. Materials and Structures 51 (110).

Zhang, S., Taheri Mousavi, S. M., Richart, N., Molinari, J.-F., Beyer, K., 2017. Micro-mechanical finite element modeling of diagonal compression test for historical stone masonry structure. International Journal of Solids and Structures 112, 122–132.